Supplementary Material for

Merlin cooperates with neurofibromin and Spred1 to suppress the Ras–Erk pathway

Yan Cui[1*], Lin Ma[1,2], Stephan Schacke[1], Jiani C. Yin[3], Yi-Ping Hsueh[4], Hongchuan Jin[5], Helen Morrison[1*]

Correspondence to: yancui.research@gmail.com or Helen.Morrison@leibniz-fli.de

This PDF file includes:

Figs. S1 to S23
Tables S1 to S3
Supplementary References

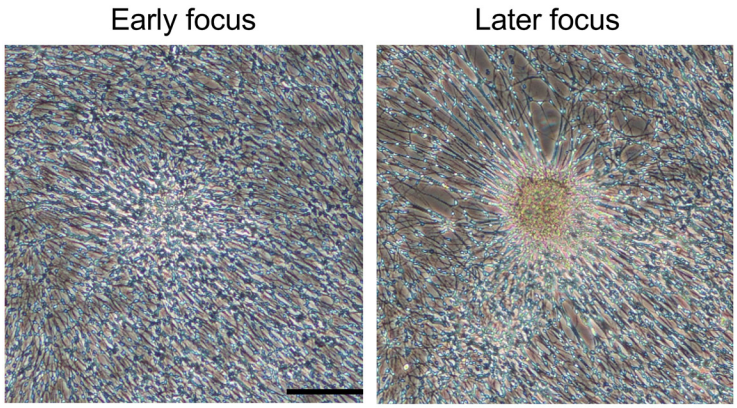

Fig. S1.

Focus formation in merlin-KD RSCs. Cells were maintained in culture for a period of ~two months. Foci could be observed after one month of culture. Scale bar, 250 μm.

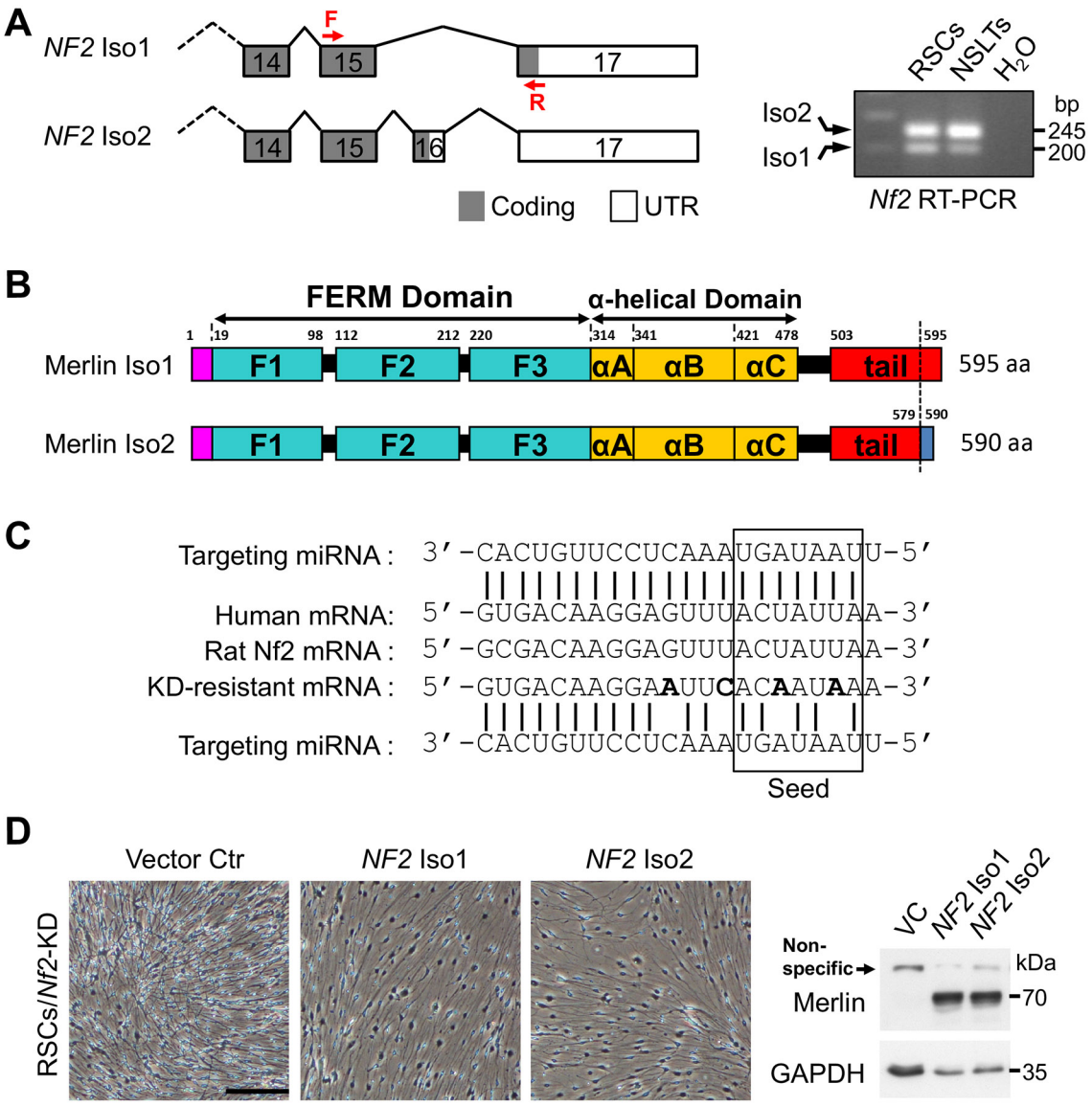

Fig. S2.

Confluent RSCs predominantly express merlin isoform 2, and both merlin isoforms can restore CICP. (**A**) Schematic diagram for the transcripts of merlin isoform 1 and 2, and their expression profiles determined by RT-PCR. Exon numbers and primer locations are indicated. (**B**) Domain organization of human merlin isoform 1 and 2. Amino acids (aa) 1–579 are identical in both isoforms; aa 1–18 are unique to merlin, not found in the related ERM (ezrin, radixin, moesin) proteins. (**C**) miRNA sequence for merlin knockdown and the KD-resistant version of merlin cDNA. (**D**) Merlin-KD RSCs (puromycin resistant) were transduced with the vector control or Strep-P-tagged merlin isoforms (KD-resistant; the vector contains blasticidin-resistant marker), selected and monitored *in situ* without passaging. Images were taken 20 days post-transduction. Strep-P: 2× Strep-tag2 followed by a PreScission Protease site. Scale bar, 250 μm.

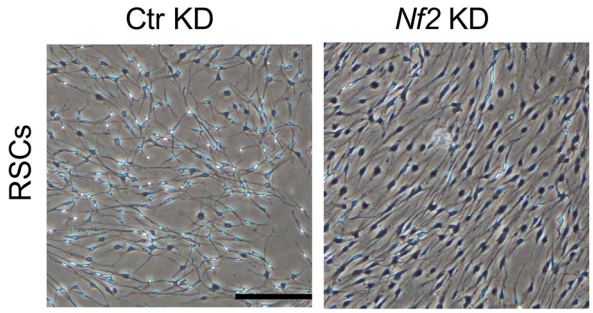

Fig. S3.

Cell status before lysis for immunoblotting, related to Fig. 1B. Cells were first amplified after transduction, then re-plated, and lysed after confluence. Scale bar, 250 µm.

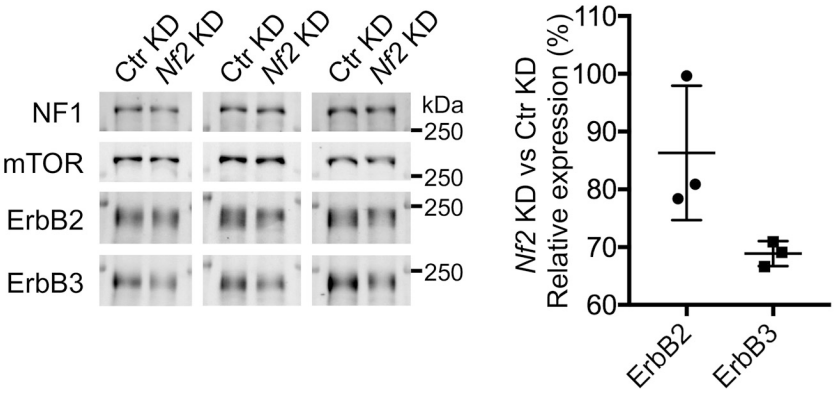

Fig. S4.

Quantification of ErbB2 and ErbB3 expression. Three replicate blots of the same batch of the samples as in Fig. 1B were quantified; each ErbB2 or ErbB3 signal was normalized to the respective mTOR signal of the same lane. ErbB2 was first probed because it had much weaker signals than ErbB3; afterwards, a short stripping was performed, which completely removed the ErbB2 signals before probing for ErbB3. See more details in the Materials and Methods section. mTOR was chosen for normalization because it had strong and clean signals, was close to ErbB2/3 on the blots, and its expression appeared not to be affected by merlin loss.

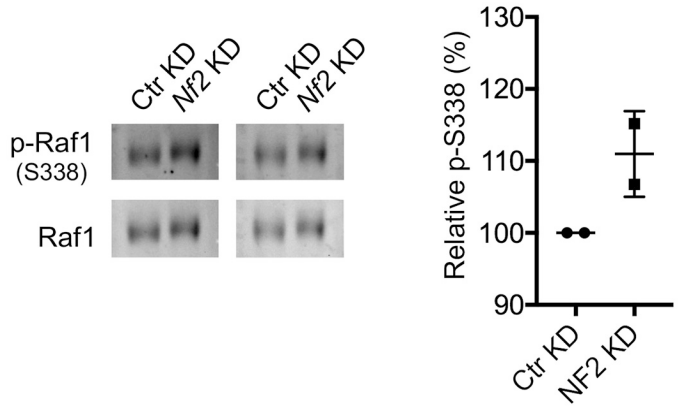

Fig. S5.

Quantification of p-Raf1 (S338) relative to the total Raf1 level. Two replicate blots of the same batch of the samples as in Fig. 1B were quantified; each p-Raf1 signal was normalized to the respective Raf1 signal of the same lane. p-Raf1 was first probed due to its relatively weak signals; afterwards, extensive wash was performed, which almost completely removed the p-Raf1 signals before probing for Raf1.

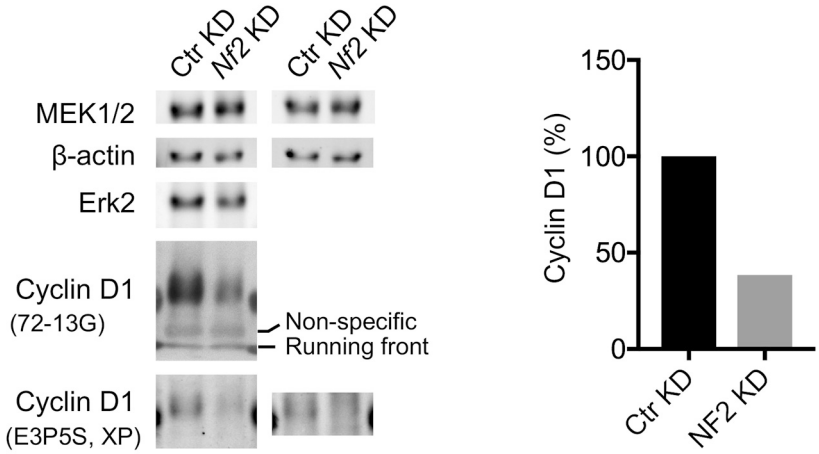

Fig. S6.

Quantification of cyclin D1 expression. The same cyclin D1 blot in Fig. 1B (probed with 72-13G) was reprobed with another cyclin D1 antibody (E3P5S). Proteins close to cyclin D1 on the blot were further probed. A replicate blot was also probed. The left blot was quantified using the signals by E3P5S, because the new results were obtained with an imager instead of films for the old results; Erk2 signals were used for normalization. E3P5S and 72-13G are from rabbit and mouse, respectively; no carry-over of the old signals was confirmed.

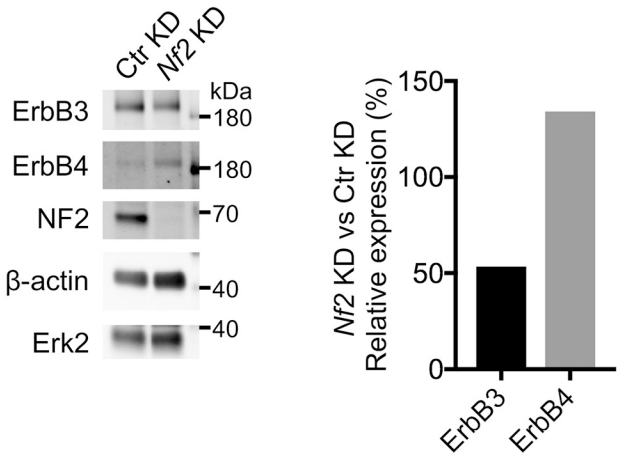

Fig. S7.

Quantification of ErbB3 and ErbB4 expression. A different batch of the samples from that in Fig. 1B was used. ErbB3 and ErbB4 signals were normalized to respective β-actin signals. ErbB4 was first probed due to its very weak signals; afterwards, a short stripping was performed, which completely removed the ErbB4 signals before probing for ErbB3.

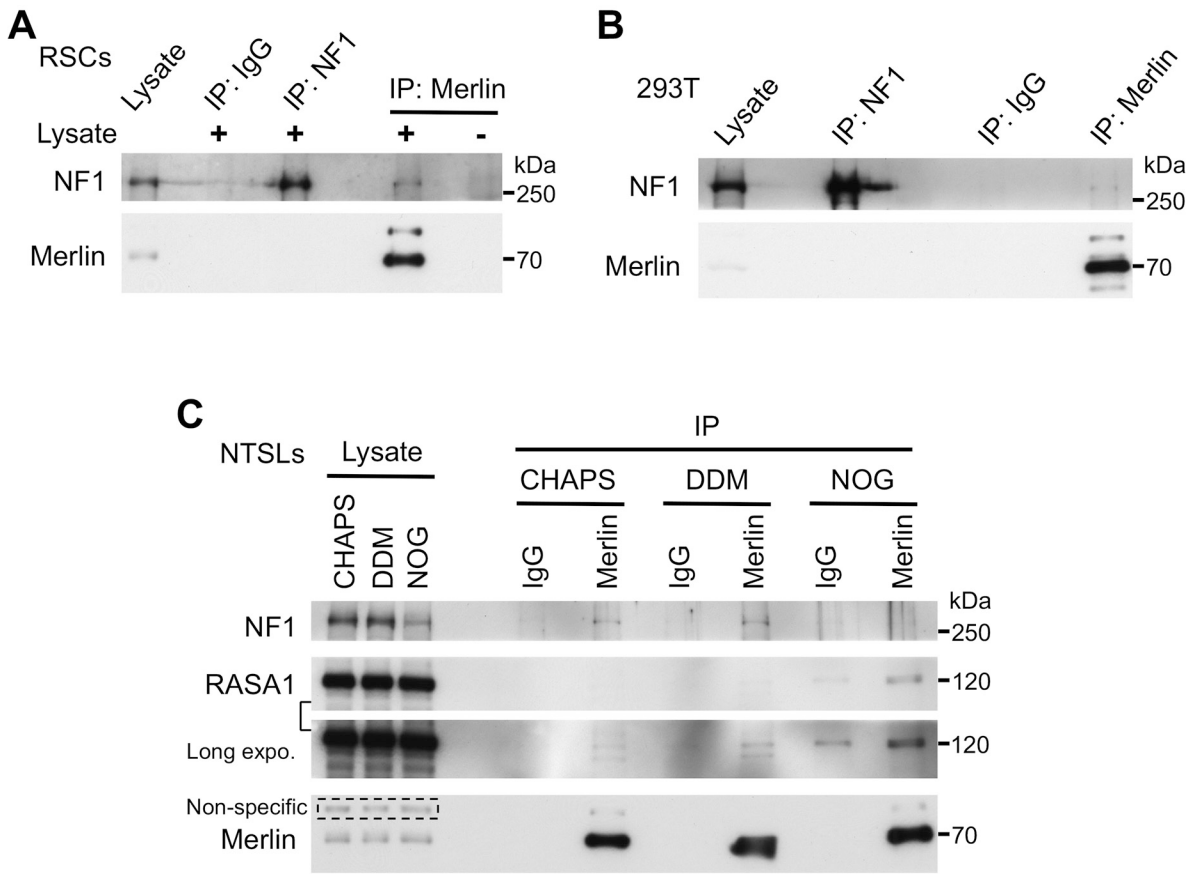

Fig. S8.

Immunoblot analysis of Co-IP of merlin and neurofibromin from indicated cell lysates. Three detergents (0.6% CHAPS, 0.1% dodecyl-β-D-maltoside [DDM], 2% n-Octyl-β-D-glucopyranoside [NOG]) were compared in (**C**).

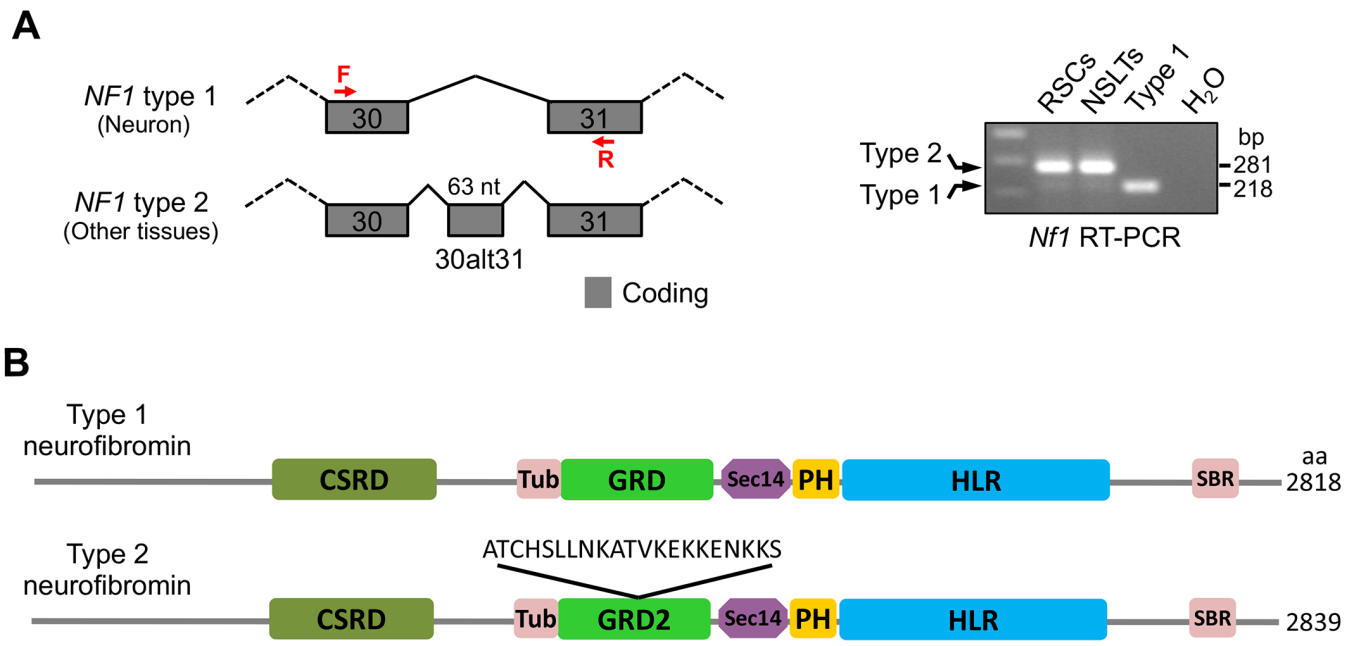

Fig. S9.

Confluent RSCs almost exclusively express neurofibromin type 2. (**A**) Schematic diagram for the transcripts of neurofibromin type 1 and 2, and their expression profiles determined by RT-PCR. A rat neurofibromin type 1 plasmid (1) was used as a PCR control. Exon numbering is according to (2). Primer locations are indicated by F and R. (**B**) Domain organization of human neurofibromin type 1 and 2, according to (3). The 21-aa insert encoded by exon 30alt31 is depicted. CSRD: Cysteine/Serine-Rich Domain; Tub: Tubulin-binding region; GRD: GAP-Related Domain; Sec14: homologous to the yeast Sec14p protein; PH: Pleckstrin Homology-like domain; HLR: HEAT-Like Repeats; SBR: Syndecan-Binding Region.

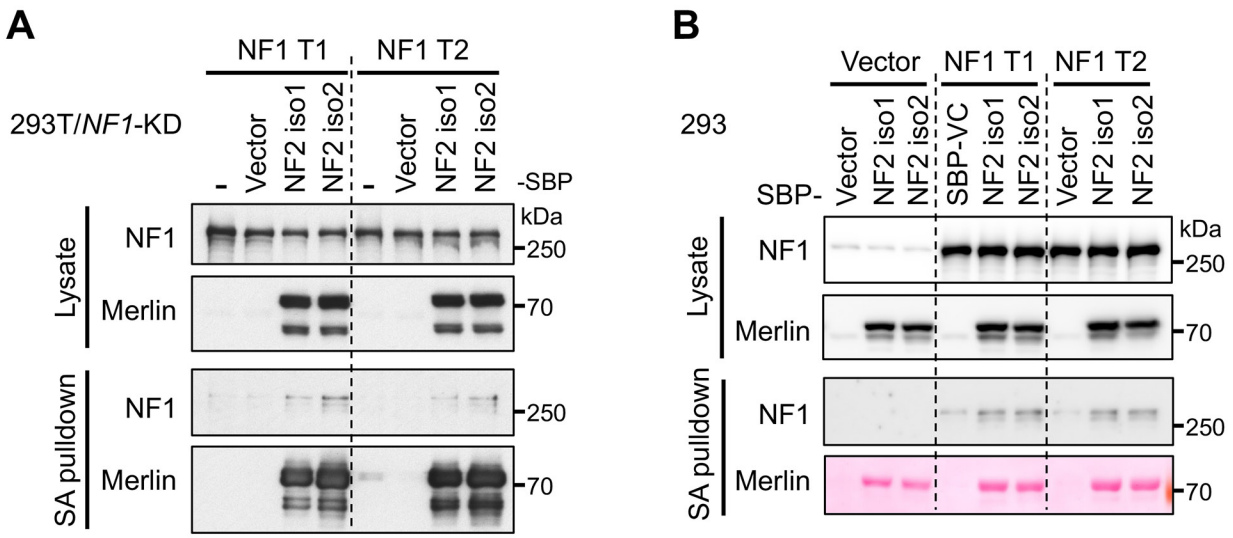

Fig. S10.

Both merlin isoforms interact with both neurofibromin isoforms. (**A, B**) Immunoblot analysis of streptavidin (SA) pulldown. (**A**) Non-tagged NF1 (under the EF1a promoter) and C-terminal SBP-tagged NF2 (wildtype, under the EFS promoter) were co-transfected into 293T/*NF1*-KD cells; ~24 h after transfection, cells were lysed for SA pulldown. (**B**) Non-tagged NF1 (under the EF1a promoter) and N-terminal SBPLL-tagged NF2 (S518A mutants, under the EFS promoter) were co-transfected into 293 cells; ~48 h after transfection, cells were lysed for SA pulldown; merlin from the pulldown was detected by Ponceau S staining. T1: type 1; T2: type 2.

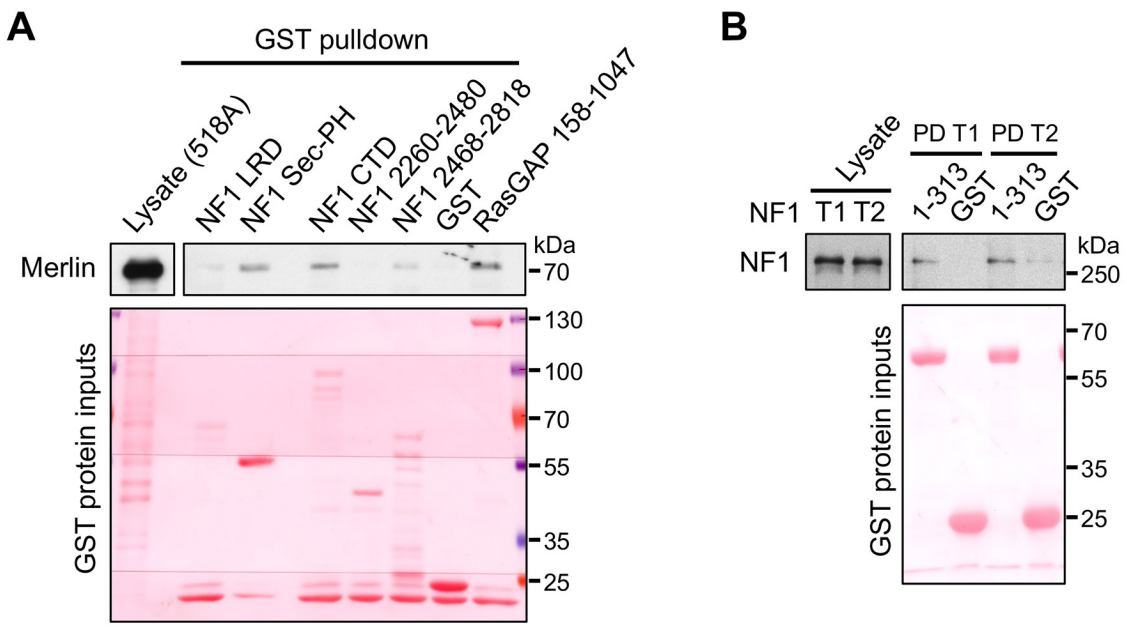

Fig. S11.

The Sec14-PH domain of neurofibromin interacts with merlin; merlin 1–313 binds to full-length neurofibromin type 1 and 2 to similar extents *in vitro*. (**A**) Immunoblot analysis of pulldown of merlin from the RT4/Tet-NF2 S518A lysate by GST-NF1 fragments. (**B**) Immunoblot analysis of pulldown of neurofibromin type 1 and 2 overexpressed in 293T/*NF1*-KD cells by GST-merlin 1–313. GST-proteins were detected by Ponceau S staining. T1: type 1; T2: type 2.

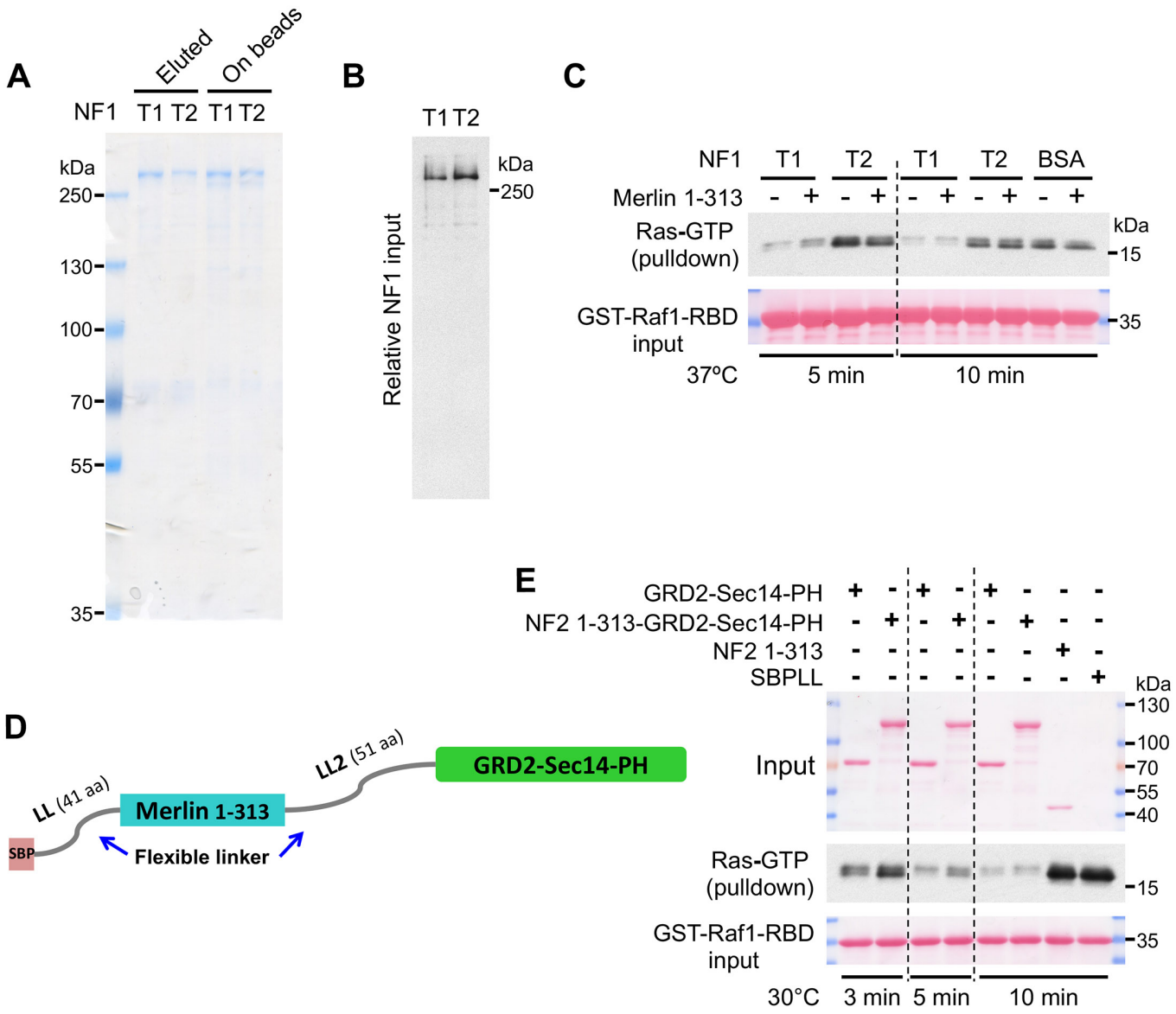

Fig. S12.

Merlin does not increase the Ras-GAP activity of neurofibromin *in vitro*. (**A**) InstantBlue staining of purified full-length neurofibromin type 1 and 2 (T1 and T2). SBP-tagged neurofibromin was purified from 293T/*NF(1+2)*-KD cells by SA pulldown, and separated by SDS-PAGE. On beads: proteins remaining on the SA agarose beads after elution with biotin. (**B**) Immunoblotting of the relative amount of neurofibromin type 1 and 2 used for the *in vitro* GAP activity assay in (C). (**C**) *In vitro* Ras-GAP activity assay by GST-Raf1 RBD pulldown. SBP-neurofibromin T1 and T2 were pre-incubated with or without SBP-merlin 1–313 on ice and used to catalyze Ras-GTP (purified HRas 1–166 preloaded with GTP) hydrolysis. BSA was used as a non-catalytic control. Reactions were assembled on ice, initialized in a 37ºC water bath, and stopped on ice. Ice-cold pulldown buffer (1 ml) was added into each reaction tube and GST-Raf1 RBD immobilized on sepharose was added to pull down the remaining Ras-GTP. Proteins were detected by immunoblotting or Ponceau S staining. (**D**) Schematic diagram of the fusion protein. (**E**) On-beads Ras-GAP activity assay. The indicated SBP-tagged protein fragments immobilized

on SA beads were used to catalyze Ras-GTP hydrolysis at 30°C on a thermomixer. Reactions were stopped on ice. Ice-cold pulldown buffer (1 ml) was added into each reaction tube, the SA beads were precipitated first, and then the supernatant was transferred to a new tube for GST-Raf1 RBD pulldown. Proteins were detected by immunoblotting or Ponceau S staining.

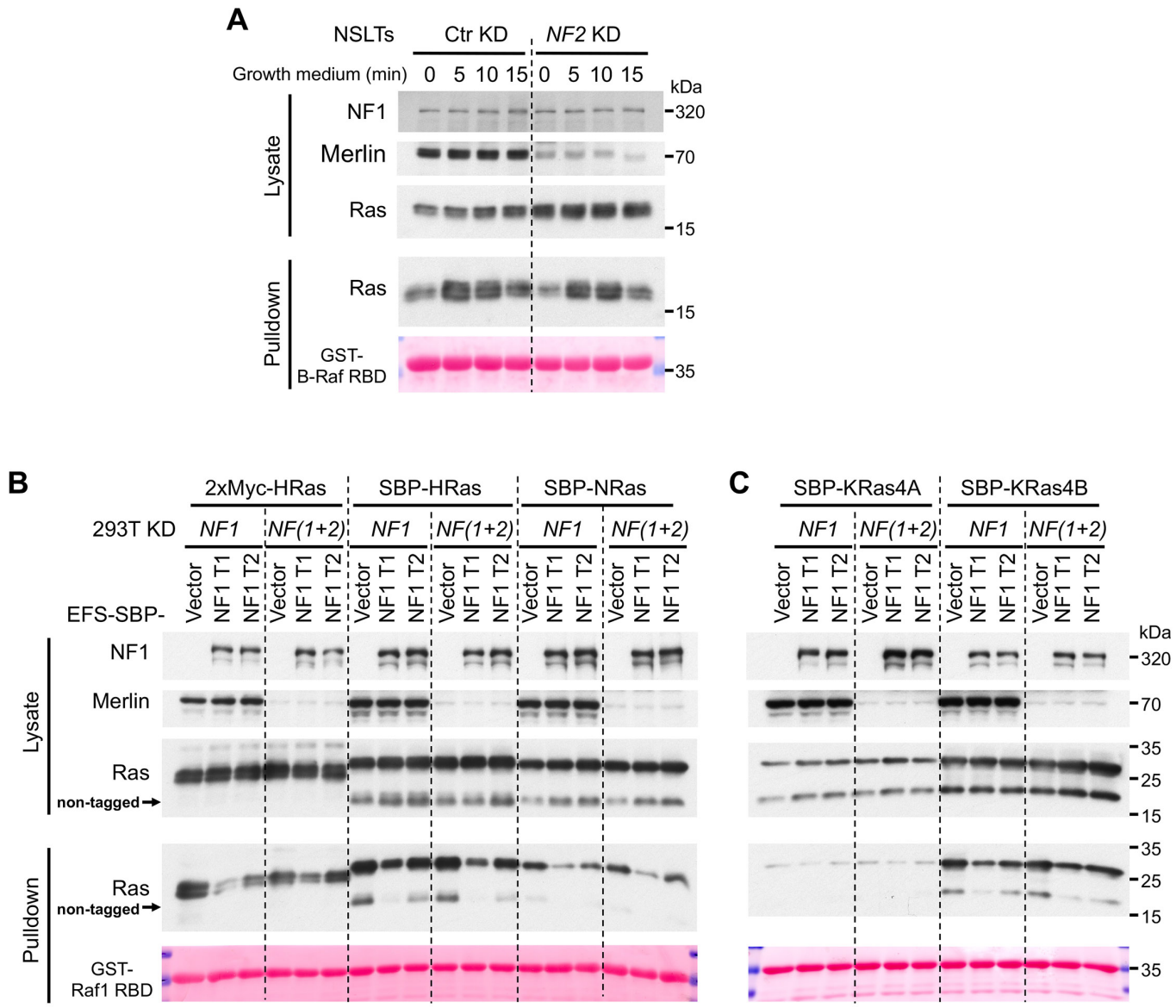

Fig. S13.

Merlin does not increase the Ras-GAP activity of neurofibromin *in vivo*. (**A**) Immunoblot analysis of endogenous Ras-GTP pulldown by GST-B-Raf RBD. NSLTs were stably transduced for knockdown and propagated. Re-seeded cells were cultured close to confluence, NRG1 starved (NRG1 omitted from the growth medium) overnight, stimulated with the growth medium for indicated time, and lysed for pulldown. (**B, C**) Immunoblot analysis of Ras-GTP (from overexpressed wildtype Ras) pulldown by GST-Raf1 RBD. Indicated Ras constructs and NF1 constructs were co-transfected into 293T/*NF1*-KD or 293T/*NF(1+2)*-KD cells; ~24 h after transfection, cells were lysed for pulldown. GST-proteins were detected by Ponceau S staining.

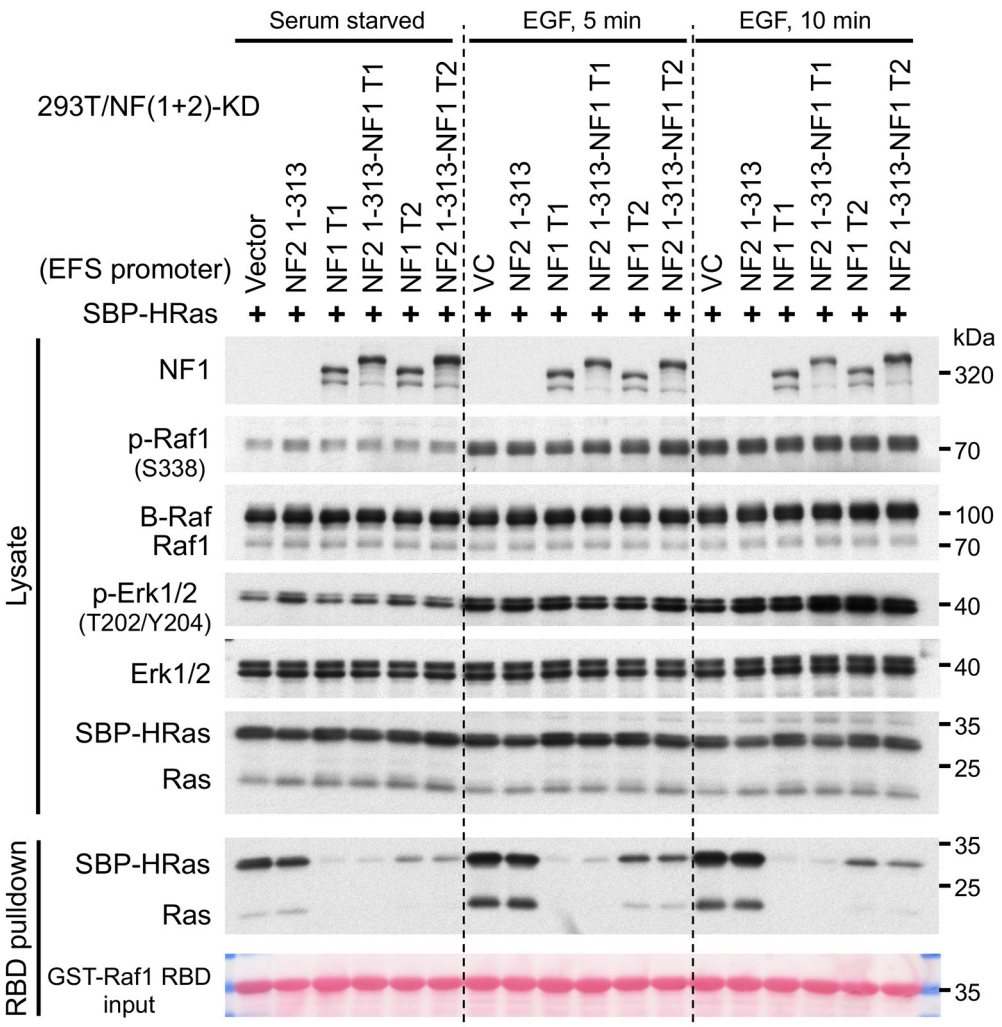

Fig. S14.

Ras-GTP level itself may not faithfully reflect its signaling output. Immunoblot analysis of HRas-GTP (from overexpressed wildtype HRas) pulldown by GST-Raf1 RBD. Indicated constructs were co-transfected into 293T/*NF(1+2)*-KD cells; ~32 h after transfection, cells were serum starved overnight; ~48 h after transfection, cells were stimulated with 20 ng/ml EGF for indicated time and lysed for pulldown. GST-proteins were detected by Ponceau S staining.

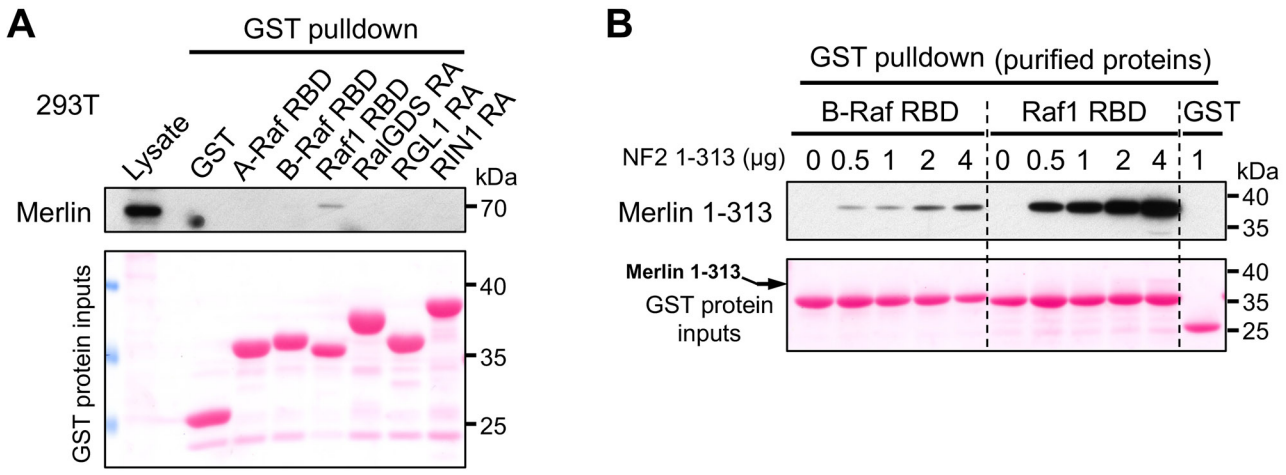

Fig. S15.

Merlin prefers Raf1 RBD over other RBD/RA domains. (**A**) Immunoblot analysis of pulldown of endogenous merlin from 293T lysate by indicated GST-RBD/RA domains. Confluent 293T cells were serum starved overnight before lysis. (**B**) Immunoblot analysis of pulldown of merlin 1–313 by indicated GST-RBDs. All proteins were purified from *E. coli*. GST-proteins were detected by Ponceau S staining. Note that merlin 1–313 in the pulldown by Raf1 RBD was also detectable by Ponceau S staining when the input was high.

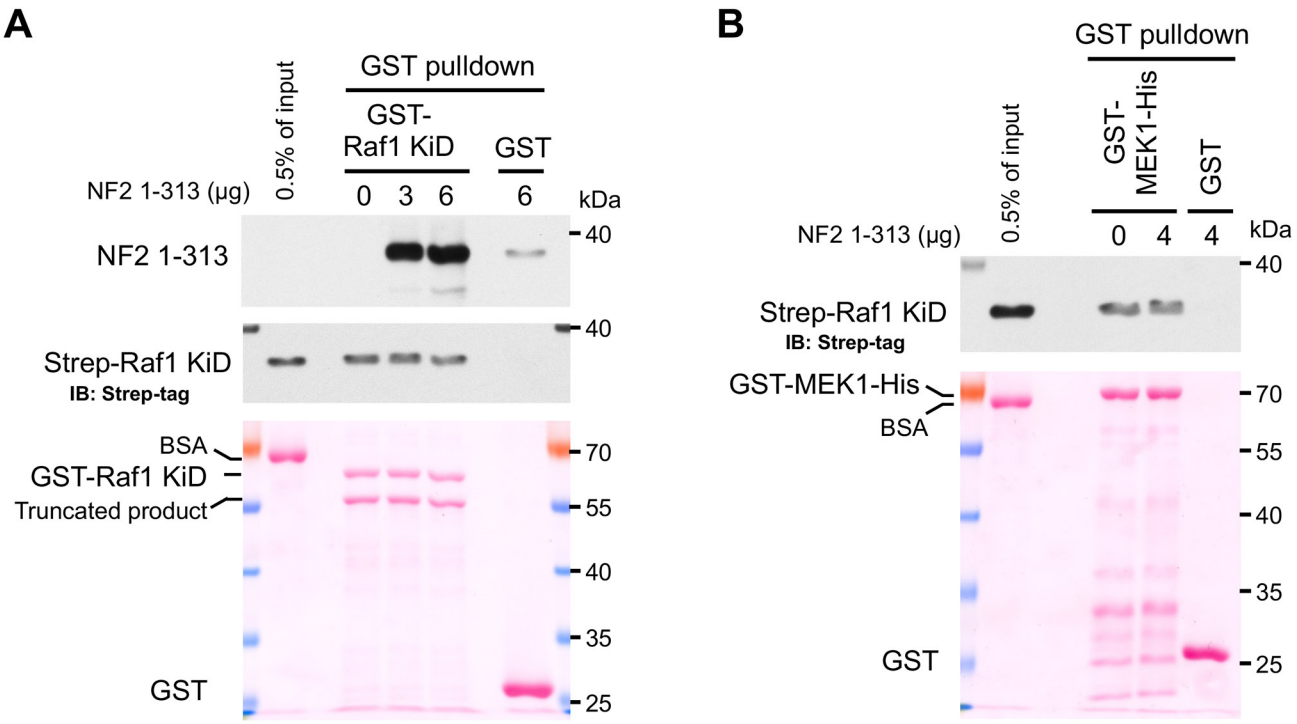

Fig. S16.

Merlin FERM does not block the isolated Raf1 KiD dimerization or interaction with MEK. (**A, B**) Immunoblot analysis of pulldown of Strept-Raf1 KiD from *E. coli* lysate by GST-Raf1 KiD (A) or GST-MEK1-His (B) in the absence or presence of merlin FERM. Note that 0.5% of input did not contain merlin 1–313. All proteins were expressed in *E. coli*. GST-proteins were detected by Ponceau S staining.

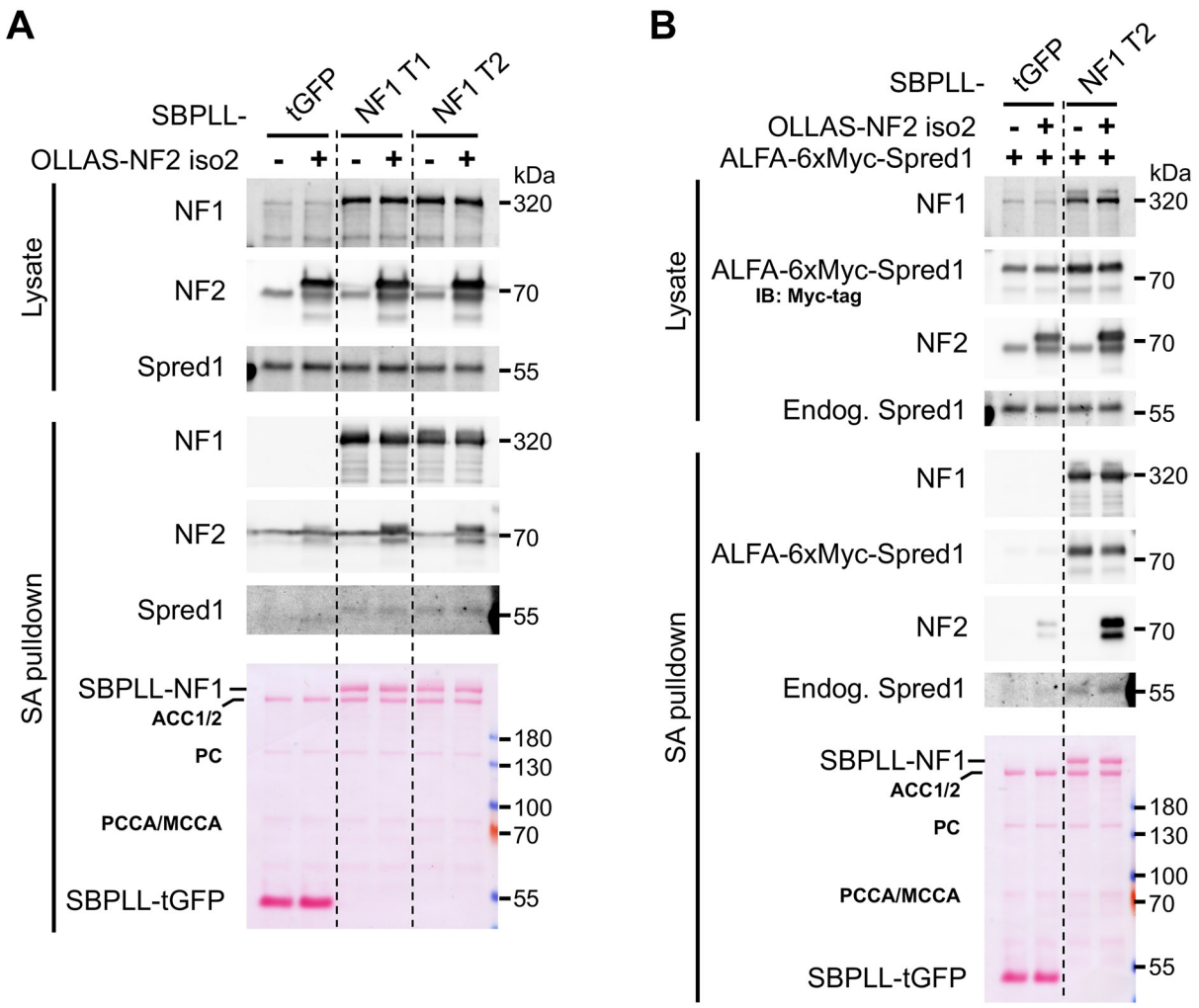

Fig. S17.

Merlin does not affect the formation of the neurofibromin/Spred1 complex. (**A and B**) Immunoblot analysis of streptavidin (SA) pulldown of SBPLL-NF1. Indicated constructs were co-transfected into 293 cells; ~24 h later, half volume of fresh medium was further added; ~48 h after transfection, cells were lysed for SA pulldown. Proteins on the blots were also detected by Ponceau S staining. The NF2 construct used the S518A mutant. Endogenously biotinylated proteins (ACC1/2, PC, PCCA/MCCA) were annotated based on their sizes. tGFP: TurboGFP; T1: type 1; T2: type 2; IB: immunoblotting

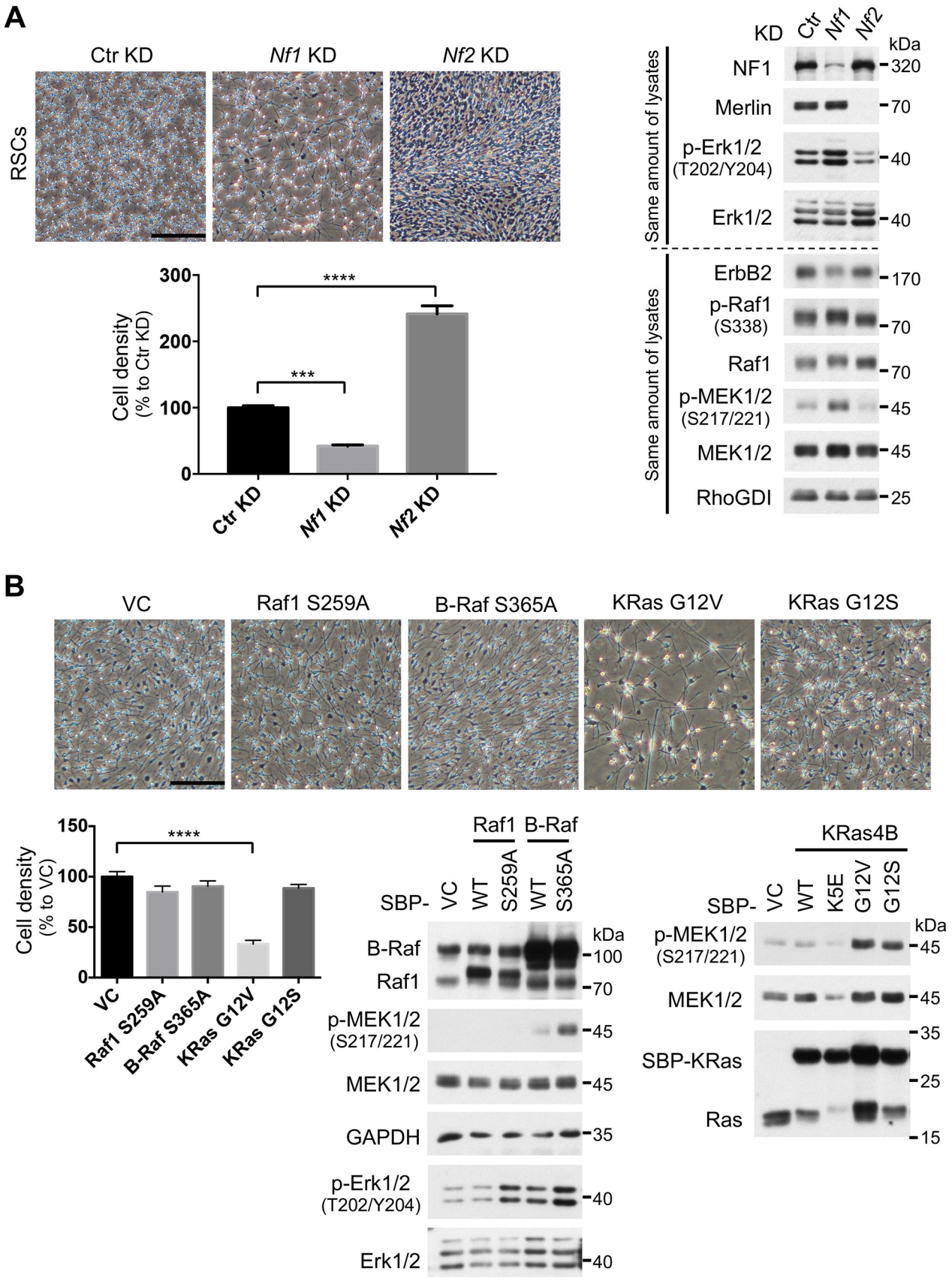

Fig. S18.

Activation of the Ras–Erk pathway is not sufficient to drive loss of CICP in RSCs. (**A**) Knockdown of *Nf1* did not increase but instead decreased the cell density. The stably transduced cells were re-

plated in equal numbers in 6-well plates in four replicates. After 21 days in culture, three replicates were counted and one lysed for immunoblotting. Cell number was normalized to that of Ctr KD and represented as mean ± SD. One-way ANOVA followed by Dunnett's multiple comparisons test was performed, ***$P \leq 0.001$; ****$P \leq 0.0001$. Of note, poly-L-lysine of mol wt 150,000–300,000 was used in this experiment as the saturation density of RSCs was higher than with poly-L-lysine of mol wt 70,000–150,000 and the trend of the relative cell density was consistent. We also performed multiple rounds of experiments in which the cells were transduced and selected *in situ* without passaging. These experiments produced similar results and the KD of *Nf1* was more complete (data not shown). The activity of the Ras–Erk pathway is highly dynamic and subject to complex regulation, heavily affected by cell densities and culture conditions. At the endpoint of this experiment, we did not observe an increased p-MEK or p-Erk level in *Nf2*-KD cells. (**B**) Overexpression of active Ras or Raf mutants did not increase cell density. KRas G12V is the classic oncogenic mutation; G12S has been found in one sporadic schwannoma (4); K5E (germline mutation) has been reported in a patient with multiple schwannomas (5); Q22R and D153V are two weakly active mutants (6) (data not shown for K5E, Q22R, and D153V). p-S259 in Raf1 (p-S365 in B-Raf) mediates the interaction with 14-3-3 proteins to stabilize the autoinhibitory conformation. The sites surrounding S259 of Raf1 are a hotspot for mutations in Noonan syndrome (7-10). Cells were transduced, selected, and monitored *in situ* without passaging. After 14 days in culture, cells were photographed and lysed for immunoblotting. Cell number was counted from at least three representative regions using Cell Counter of ImageJ. Cell number was normalized to that of the VC (vector control) and represented as mean ± SD. One-way ANOVA followed by Dunnett's multiple comparisons test was performed, ****$P \leq 0.0001$. Representative results of two independent experiments are shown. None of the tested mutants increased the cell density. Scale bars, 250 μm.

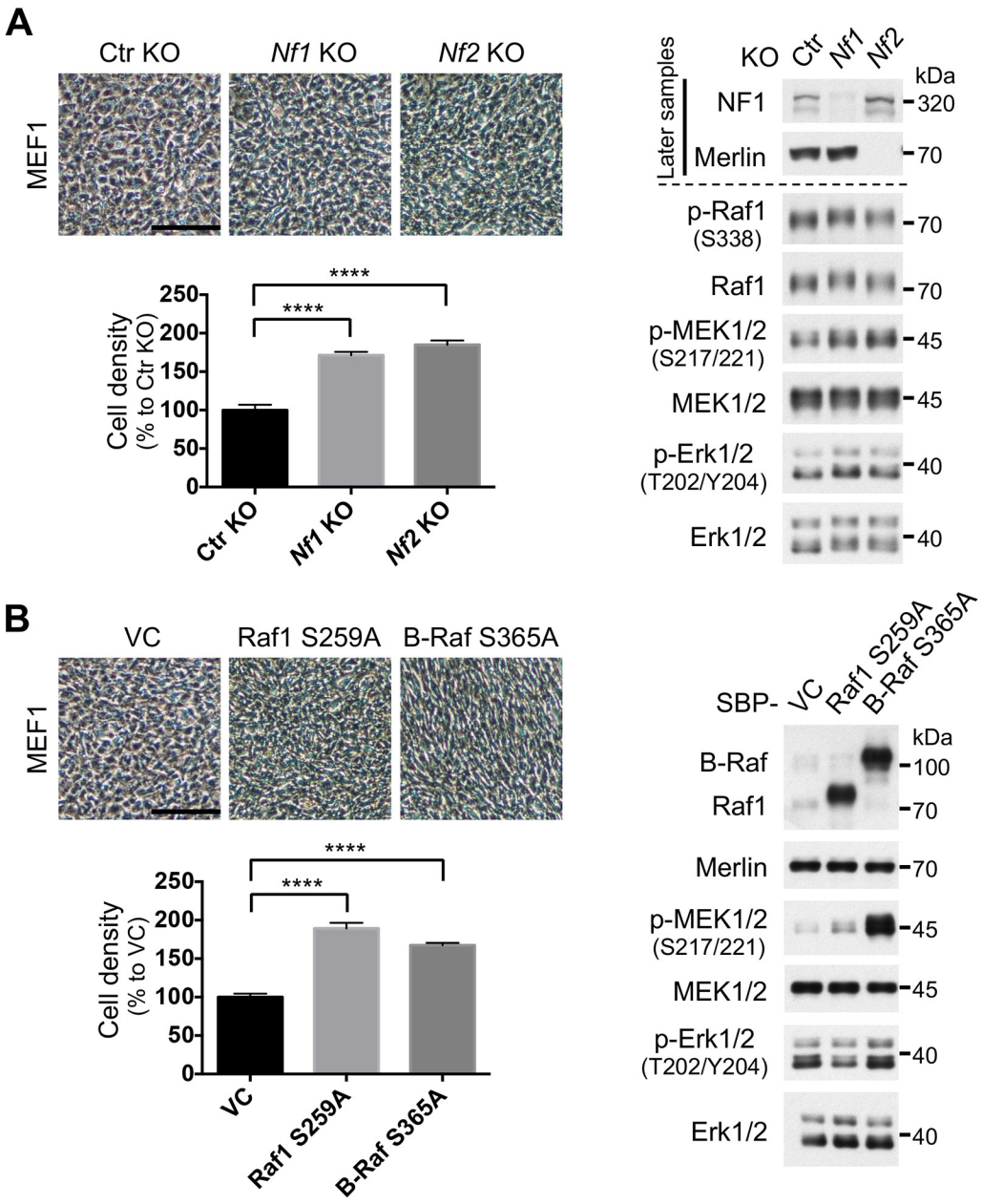

Fig. S19.

Activation of the Ras–Erk pathway drives loss of CICP in an immortalized MEF line. MEF1 is a spontaneously immortalized MEF line (11) showing characteristic CICP in extended culture. (**A**) Knockout (KO) of *Nf1* or *Nf2* by lentiviral CRISPR/Cas9 vectors in MEF1. Cells were transduced in triplicate, selected, and monitored *in situ* without passaging. After 16 days in culture, cells were photographed and trypsinized for counting. A portion of the remaining cells was re-plated for amplification and the rest were pelleted for immunoblotting. Cell number was normalized to that of control KO and represented as mean ± SD. One-way ANOVA followed by Dunnett's multiple comparisons test was performed, ****$P \leq 0.0001$. Representative results of two independent experiments are shown. We also used a second sgRNA to knockout *Nf1* and *Nf2* and similar results were obtained (data not shown). (**B**) Overexpression of active Raf mutants in MEF1. Stably transduced cells were re-plated in equal numbers in 6-well plates in triplicate. Cells were cultured for 8 days before being

photographed and trypsinized for counting. Cell number was normalized to that of vector control (VC) and represented as mean ± SD. One-way ANOVA followed by Dunnett's multiple comparisons test was performed, ****$P \leq 0.0001$. Representative results of two independent experiments are shown. Of note, the immunoblotting was to validate the expression of the Raf mutants after amplifying the stably transduced cells (not the same conditions as for the counting). Also, in Raf1 S259A-expressing cells, increased p-MEK, but not increased p-Erk, was more consistently observed under the normal culture condition (no serum starvation/stimulation), probably due to the different activation kinetics of MEK and Erk. Scale bars, 250 μm.

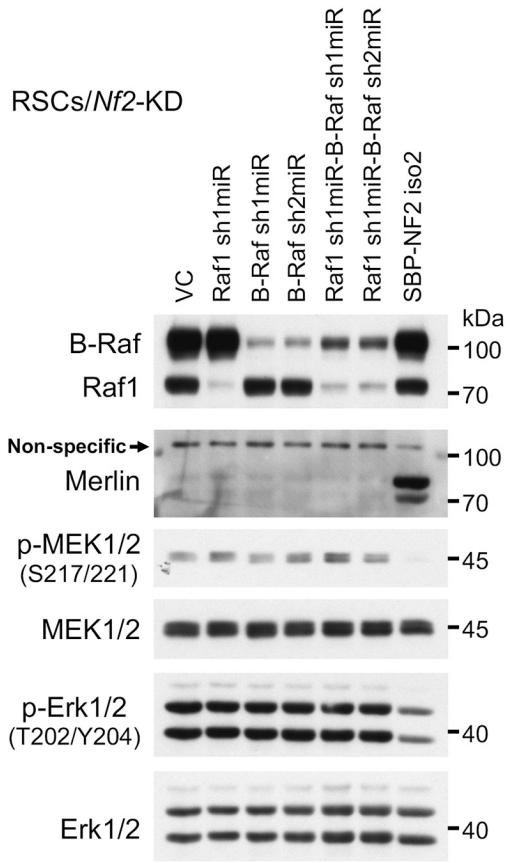

Fig. S20.

Knockdown of Raf fails to reduce the basic activity of MEK or Erk in merlin-KD RSCs. Cells were transduced, selected, and monitored *in situ* without passaging. After 11 days in culture, cells were photographed and lysed for immunoblotting. Of note, the knockdown efficiency was reasonable but incomplete. Also, as various feedback regulations exist in the Ras–Erk pathway, this may help to explain why the cells could adapt to the knockdown.

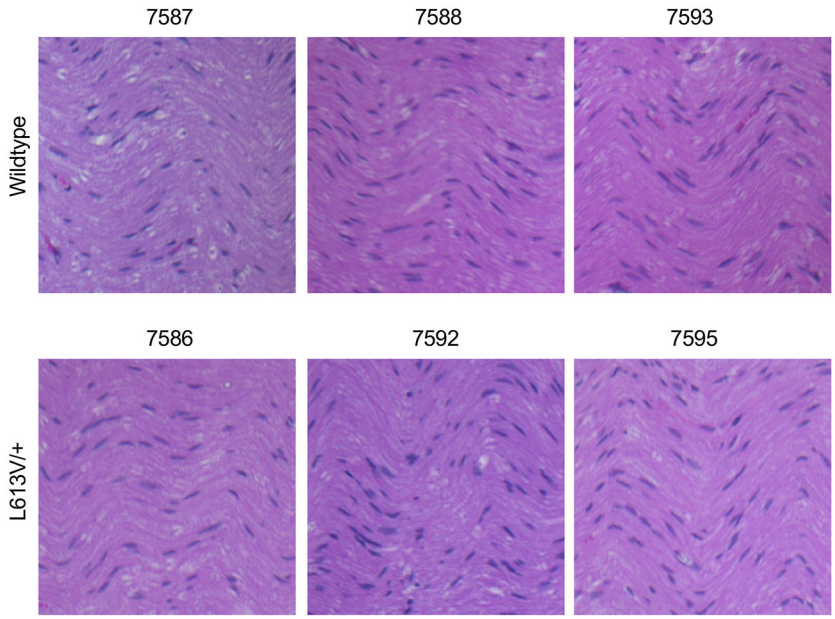

Fig. S21.

The Raf1 L613V/+ mice show normal sciatic nerves. HE staining of sciatic nerves from 14-week-old Raf1 L613V/+ mice (129Sv × C57BL/B6; n = 6) and the wildtype littermates (n = 4). Pictures from three animals of each genotype are shown. Numbers denote the respective animal number.

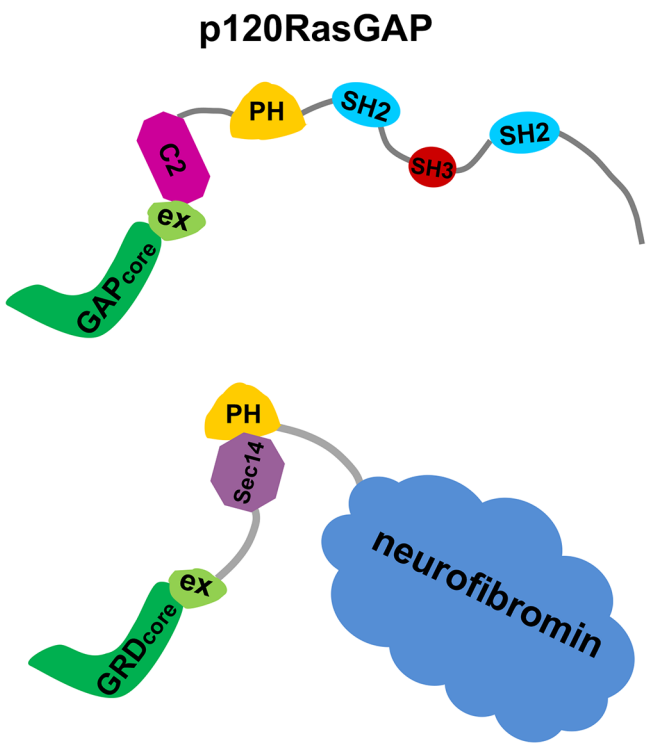

Fig. S22.

PH-C2 in p120RasGAP and Sec14-PH in neurofibromin take a similar position relative to the GAP domain or GRD.

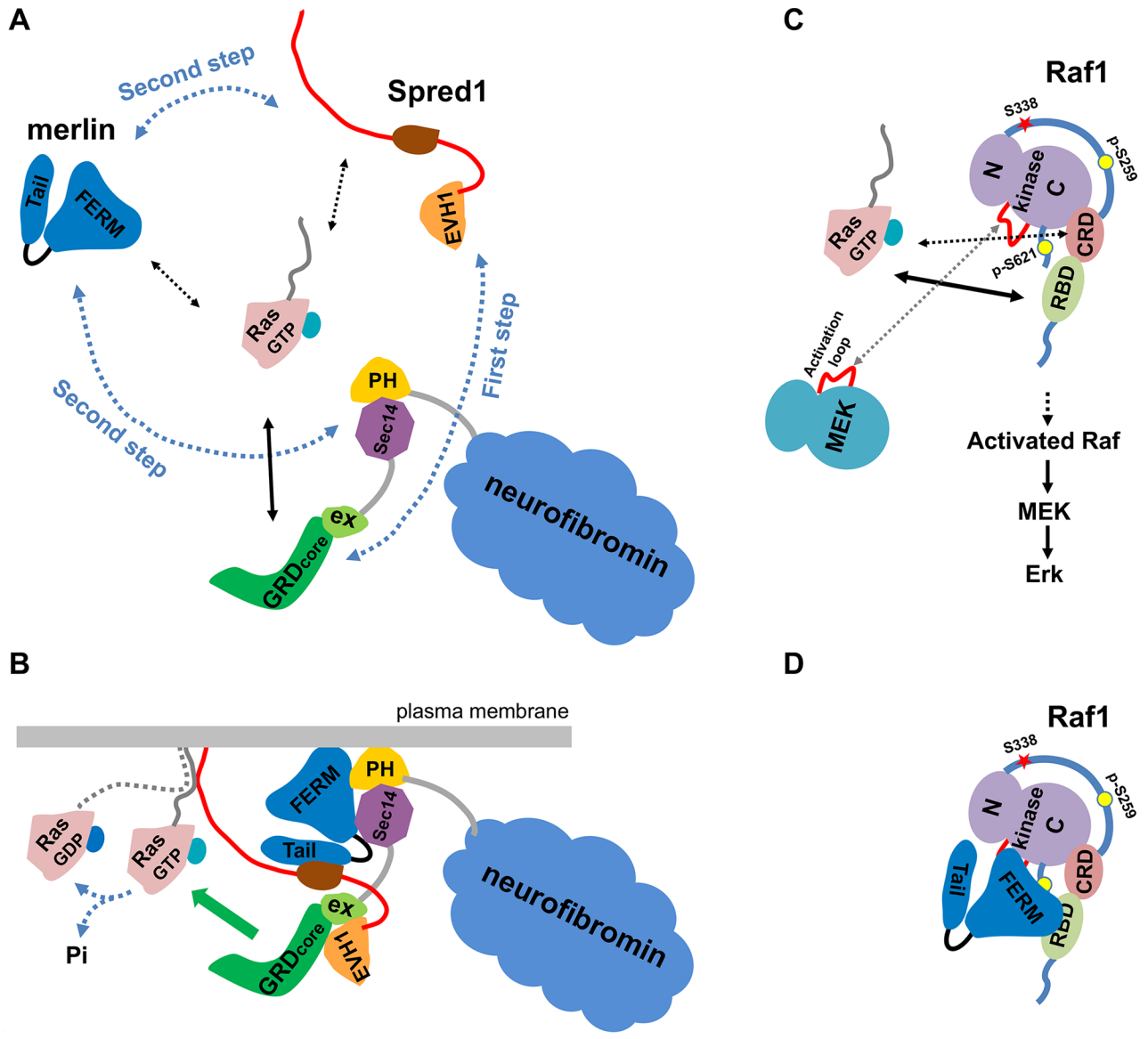

Fig. S23.

Model in which merlin cooperates with neurofibromin and Spred1 to suppress the Ras–Erk pathway. (**A, B**) Merlin, neurofibromin, and Spred1 can interact with each other and also with Ras. GRD prefers to bind to GTP-loaded Ras and accelerates Ras-GTP conversion into Ras-GDP. Neurofibromin and Spred1 form a complex first because of the high affinity between the EVH1 domain and the GRD, then merlin join. GRD here refers to both type 1 and 2. Neurofibromin likely exists as a homo-dimer (12, 13); for simplicity, only a monomer is depicted. (**C**) The autoinhibited conformation of Raf1, which is susceptible to activation mediated by Ras-GTP binding. The CRD and a 14-3-3 dimer that simultaneous binds to p-S259 and p-S621 mediate the autoinhibition. Ras-GTP binds to the RBD-CRD unit, with RBD being the high affinity site. The RBD and most of the CRD are accessible by Ras. The interface for MEK binding is also freely accessible. For simplicity, a 14-3-3 protein dimer is not depicted. Phosphorylation of S338 is critical for Raf1 activation (14). N: N-lobe; C: C-lobe. (**D**) Merlin binds to the RBD and the kinase domain of Raf1. Merlin's binding to RBD can blocks Ras-GTP binding; merlin's binding to the kinase domain likely stabilizes the merlin/Raf1 complex and the autoinhibitory conformation of Raf1.

Merlin likely interacts with Raf1, Ras and the neurofibromin/Spred1 complex in a highly dynamic way. Merlin appears to slightly interfere with the Ras-GAP activity of neurofibromin, but more importantly functions as a “selective Ras barrier” to suppress Raf1 activation. In the absence of merlin, although neurofibromin can efficiently inactivate Ras-GTP, Ras-GTP-mediated Raf1 activation may not be efficiently prevented. Of note, merlin likely acts at multiple levels to suppress the Ras–Erk pathway, which has been discussed in (15).

Table S1.

Antibodies used in this study.

Antibody	Clone/ID	Cat. No.	Supplier	Use
Akt		9272	Cell Signaling	IB
Akt1/2/3	H-136	sc-8312	Santa Cruz	IB
β-Actin	AC-15	A5441	Sigma-Aldrich	IB
Cyclin D1	72-13G	sc-450	Santa Cruz	IB
Cyclin D1	E3P5S (XP)	55506	Cell Signaling	IB
EGFR	A-10	sc-373746	Santa Cruz	IB
Erk 2	K-23	sc-153	Santa Cruz	IB
FGFR1	D8E4 (XP)	9740	Cell Signaling	IB
GAPDH	6C5	sc-32233	Santa Cruz	IB
GFP	D5.1 (XP)	2956	Cell Signaling	IB
HER2/ErbB2	D8F12 (XP)	4290	Cell Signaling	IB
HER3/ErbB3	D22C5 (XP)	12708	Cell Signaling	IB
HER4/ErbB4	111B2	4795	Cell Signaling	IB
IGF-1Rβ	D23H3 (XP)	9750	Cell Signaling	IB
MEK1/2	D1A5	8727	Cell Signaling	IB
MEK1/2	EPR16667	ab178876	Abcam	IB
Merlin	D6N8H	12896	Cell Signaling	IB
Merlin	D1D8	6995	Cell Signaling	IB
Merlin	B-12	sc-55575	Santa Cruz	IB
Merlin	AF1G4	ab88957	Abcam	IB
Merlin	A-19	sc-331	Santa Cruz	IB, IP
mTOR	7C10	2983	Cell Signaling	IB
Myc-tag	9B11	2276	Cell Signaling	IB
Neurofibromin	H12	sc-376886	Santa Cruz	IB
Neurofibromin	D	sc-67	Santa Cruz	IB, IP
p-Akt (S473)	D9E (XP)	4060	Cell Signaling	IB
p-c-Raf (S259)		9421	Cell Signaling	IB
p-c-Raf (S338)	56A6	9427	Cell Signaling	IB
p-EGFR (Y1068)	D7A5 (XP)	3777	Cell Signaling	IB
p-ErbB3 (Y1289)	EPR2325	2526-1	Epitomics	IB
p-ErbB4 (Y1284)	EPR2273(2)	3412-1	Epitomics	IB
p-Erk1/2 (T202/Y204)	D13.14.4E (XP)	4370	Cell Signaling	IB
p-MEK1/2 (S217/221)	41G9	9154	Cell Signaling	IB
p-p38 MAPK (T180/Y182)	D3F9 (XP)	4511	Cell Signaling	IB
p-p70 S6K α (T389)		sc-11759-R	Santa Cruz	IB

p38 MAPK	D13E1 (XP)	8690	Cell Signaling	IB
p70 S6K		9202	Cell Signaling	IB
PDGFR-β	985	sc-432	Santa Cruz	IB
Raf-B	F-7	sc-5284	Santa Cruz	IB
Raf1	C-12	sc-133	Santa Cruz	IB
Raf1	53/c-Raf-1	610152	BD Biosciences	IB
Ras	From the Kit	16117	Pierce	IB
Ras	EP1125Y	ab52939	Abcam	IB
Ras	RAS10	05-516	Sigma-Aldrich	IB
RasGAP	13/RAS-GAP	610040	BD Biosciences	IB
Rho GDIα	A-20	sc-360	Santa Cruz	IB
Spred1	D6D8B	94063	Cell Signaling	IB
Strep-tag2	StrepMAB-Immo	2-1517-001	IBA	IB
Goat anti-Rabbit IgG-HRP		P0448	Dako	IB
Goat anti-Mouse IgG-HRP		P0447	Dako	IB
Donkey anti-Mouse IgG-IRDye 800CW		926–32212	LI-COR	IB
Donkey anti-Rabbit IgG-IRDye 800CW		926–32213	LI-COR	IB

IB: immunoblotting; IP: immunoprecipitation.

Table S2.

Target sequences for knockdown.

Gene	KD vector	Target sequence	Target species
NF1	sh1	gctggcagtttcaaacgtaa	Human, mouse, rat, *et al.*
NF2	sh1	gtgacaaggagtttactattaa	Human, mouse, rat, *et al.*
Raf1	sh1	tgttgcagtaaagatcctaaa	Human, mouse, rat, *et al.*
	sh2	agtggttctcagcaggttgaa	Human, mouse, rat, *et al.*
B-Raf	sh1	accaaatttgagatgatcaaa	Human, mouse, rat, *et al.*
	sh2	ccacagagacctcaagagtaa	Human, mouse, rat, *et al.*

Table S3.

Oligo sequences for CRISPR/Cas9-mediated knockout.

Gene	Oligo	Sequence	Target species
Hras	sgIntr-T	cacc gctgggttgacatagctcca	Rat (intron region, served as a control)
	sgIntr-B	aaac tggagctatgtcaacccagc	
Nf1	sg1-T	cacc gtcacaatgatgggagacc	Mouse, rat
	sg1-B	aaac ggtctcccatcattgtgac	
Nf2	sg1-T	cacc gtatacaatcaaggacacgg	Mouse, rat
	sg1-B	aaac ccgtgtccttgattgtatac	

Supplementary References

1 Suzuki, H., Takahashi, K., Yasumoto, K. and Shibahara, S. (1994) Activation of the tyrosinase gene promoter by neurofibromin. *Biochem. Biophys. Res. Commun.*, **205**, 1984-1991.

2 Anastasaki, C., Le, L.Q., Kesterson, R.A. and Gutmann, D.H. (2017) Updated nomenclature for human and mouse neurofibromatosis type 1 genes. *Neurol. Genet.*, **3**, e169.

3 Bonneau, F., Lenherr, E.D., Pena, V., Hart, D.J. and Scheffzek, K. (2009) Solubility survey of fragments of the neurofibromatosis type 1 protein neurofibromin. *Protein Expr. Purif.*, **65**, 30-37.

4 Serrano, C., Simonetti, S., Hernandez-Losa, J., Valverde, C., Carrato, C., Bague, S., Orellana, R., Somoza, R., Moline, T., Carles, J. *et al.* (2013) BRAF V600E and KRAS G12S mutations in peripheral nerve sheath tumours. *Histopathology*, **62**, 499-504.

5 Bertola, D.R., Pereira, A.C., Brasil, A.C., Suzuki, L., Leite, C., Falzoni, R., Tannuri, U., Poplawski, A.B., Janowski, K.M., Kim, C.A. *et al.* (2012) Multiple, diffuse schwannomas in a RASopathy phenotype patient with germline KRAS mutation: a causal relationship? *Clin. Genet.*, **81**, 595-597.

6 Gremer, L., Merbitz-Zahradnik, T., Dvorsky, R., Cirstea, I.C., Kratz, C.P., Zenker, M., Wittinghofer, A. and Ahmadian, M.R. (2011) Germline KRAS mutations cause aberrant biochemical and physical properties leading to developmental disorders. *Hum. Mutat.*, **32**, 33-43.

7 Pandit, B., Sarkozy, A., Pennacchio, L.A., Carta, C., Oishi, K., Martinelli, S., Pogna, E.A., Schackwitz, W., Ustaszewska, A., Landstrom, A. *et al.* (2007) Gain-of-function RAF1 mutations cause Noonan and LEOPARD syndromes with hypertrophic cardiomyopathy. *Nat. Genet.*, **39**, 1007-1012.

8 Razzaque, M.A., Nishizawa, T., Komoike, Y., Yagi, H., Furutani, M., Amo, R., Kamisago, M., Momma, K., Katayama, H., Nakagawa, M. *et al.* (2007) Germline gain-of-function mutations in RAF1 cause Noonan syndrome. *Nat. Genet.*, **39**, 1013-1017.

9 Kobayashi, T., Aoki, Y., Niihori, T., Cave, H., Verloes, A., Okamoto, N., Kawame, H., Fujiwara, I., Takada, F., Ohata, T. *et al.* (2010) Molecular and clinical analysis of RAF1 in Noonan syndrome and related disorders: dephosphorylation of serine 259 as the essential mechanism for mutant activation. *Hum. Mutat.*, **31**, 284-294.

10 Molzan, M., Schumacher, B., Ottmann, C., Baljuls, A., Polzien, L., Weyand, M., Thiel, P., Rose, R., Rose, M., Kuhenne, P. *et al.* (2010) Impaired binding of 14-3-3 to C-RAF in Noonan syndrome suggests new approaches in diseases with increased Ras signaling. *Mol. Cell. Biol.*, **30**, 4698-4711.

11 Zhou, Z.W., Liu, C., Li, T.L., Bruhn, C., Krueger, A., Min, W., Wang, Z.Q. and Carr, A.M. (2013) An essential function for the ATR-activation-domain (AAD) of TopBP1 in mouse development and cellular senescence. *PLoS Genet.*, **9**, e1003702.

12 Carnes, R.M., Kesterson, R.A., Korf, B.R., Mobley, J.A. and Wallis, D. (2019) Affinity Purification of NF1 Protein-Protein Interactors Identifies Keratins and Neurofibromin Itself as Binding Partners. *Genes (Basel)*, **10**.

13 Sherekar, M., Han, S.W., Ghirlando, R., Messing, S., Drew, M., Rabara, D., Waybright, T., Juneja, P., O'Neill, H., Stanley, C.B. *et al.* (2020) Biochemical and structural analyses reveal that the tumor suppressor neurofibromin (NF1) forms a high-affinity dimer. *J. Biol. Chem.*, **295**, 1105-1119.

14 Matallanas, D., Birtwistle, M., Romano, D., Zebisch, A., Rauch, J., von Kriegsheim, A. and Kolch, W. (2011) Raf family kinases: old dogs have learned new tricks. *Genes Cancer*, **2**, 232-260.

15 Cui, Y., Groth, S., Troutman, S., Carlstedt, A., Sperka, T., Riecken, L.B., Kissil, J.L., Jin, H. and Morrison, H. (2019) The NF2 tumor suppressor merlin interacts with Ras and RasGAP, which may modulate Ras signaling. *Oncogene*, **38**, 6370-6381.